Ion beam instability model for the Mercury upstream waves

Yasuhito Narita[1,2,*], Daniel Schmid[3,*], and Uwe Motschmann[1,*]

[1]Institut für Theoretische Physik, Technische Universität Braunschweig, Mendelssohnstr. 3, D-38106 Braunschweig, Germany

[2]Max Planck Institute for Solar System Research, Justus-von-Liebig-Weg 3, D-37077 Göttingen, Germany

[3]Space Research Institute, Austrian Academy of Sciences, Schmiedlstr. 6, 8042 Graz, Austria

[*]These authors contributed equally to this work.

Correspondence: Y. Narita (y.narita@tu-braunschweig.de)

Abstract. An analytic model for the ion beam instability is constructed in view of application to the Mercury upstream waves. Our ion beam instability model determines the frequency and the wavenumber by equating the whistler dispersion relation with the beam resonance condition in favor of planetary foreshock wave excitation. By introducing the Doppler shift in the instability frequency, our model can derive the observer-frame relation of the resonance frequency to the beam velocity and the flow speed. The frequency relation serves as a useful diagnostic tool to the Mercury upstream wave studies in the upcoming BepiColombo observations.

1 Introduction

Upstream region of the Mercury bow shock is unique in the plasma physical sense in that the low-frequency electromagnetic waves are excited in the nearly radial interplanetary to the Sun and in a moderate Mach number flow below 10. Diffuse and field-aligned beam and the low-frequency waves are detected by the MESSENGER spacecraft (e.g., Le et al., 2013; Romanelli and DiBraccio, 2021; Glass et al., 2023), mechanism of which is reminiscent of the Earth foreshock formation Naive calculation gives a Parker spiral angle of about 20 degree to the radial direction to the Sun. The MESSENGER magnetic field and the ENLIL model calculation estimate the flow speed is about 350–400 $\mathrm{km\,s^{-1}}$, which corresponds to an Alfvén Mach number around 6.

Various kinds of low-frequency electromagnetic waves are observed upstream of the Mercury bow shock by the MESSENGER spacecraft such as whistler mode at about 2 Hz (in the spacecraft frame), fast mode wave at about 0.3 Hz (Le et al., 2013), and ion-cyclotron associated with the pickup protons (Schmid et al., 2022). Here we propose that the right-hand resonant instability driven by the beam ions can explain both the whistler/magnetosonic mode below or around the ion cyclotron frequency (for protons) such as the waves at 0.3 Hz in the spacecraft frame (cf. proton cyclotron frequency is about 0.46 Hz for a magnetic field magnitude of 30 nT) and the pickup ion cyclotron waves. The wave excitation at higher frequency such as at 2 Hz in the spacecraft frame needs a modification of our model such as an anti-sunward streaming ion beam in the observer frame, parametric instabilities, or a sunward streaming electron beam. The lesson from the Earth foreshock studies is that the foreshock waves are driven by the shock-reflected, back-streaming ions interacting with the solar wind, and the waves are driven by the right-hand resonant ion beam instability, also referred to as the component-component instability (Gary, 1993). The pickup ion cyclotron waves are unique to the extended exospheric region such that the neutral species (atomic hydrogen) is photo-ionized in interplanetary space, and are observed around Mercury (Schmid et al., 2022) as well as Venus and Mars (Delva et al., 2011a, b).

Both the foreshock and ion-cyclotron waves exhibit left-hand field rotation about the mean magnetic field in the temporal sense when seen in the spacecraft frame, because the right-hand beam resonance undergoes a Doppler shift in the opposite direction to the beam and the wave polarization is reversed into left-hand rotation sense. The pickup ion cyclotron waves are also observed as a left-handed field rotation sense because the spacecraft frame is virtually the same as the rest frame of pickup ions.

We develop an analytic model of the ion beam instability relevant to the Mercury upstream waves in view of the upcoming arrival of the BepiColombo mission at Mercury (Benkhoff et al., 2021). Our foreshock model is constructed of the dispersion relation of whistler waves and the beam resonance condition. We derive a constraint relation between the frequency (or wavenumber) of the instability, the beam velocity, and the flow speed. The model has a capability to estimate the flow speed if the beam velocity is known or assumed, or vice verse to estimate the beam velocity if the flow speed is known or assumed. In particular, the Mio spacecraft of BepiColombo covers a wide range of radial distance to Mercury up to about 6 planetary radii, which is suited to perform a systematic survey of the Mercury upstream waves with the magnetometer and plasma detectors. Our model serves as a diagnostic tool to determine or constraint the velocities (flow speed and beam velocity) even using the magnetic field data.

2 Resonance frequency estimate

2.1 Problem setup

In the theoretical framework, the beam instability is conveniently analyzed in the rest frame of the bulk plasma. We refer to this frame as the flow frame, comoving with the solar wind. The ion beam is injected into the system at a speed of U_{b} (the beam direction is taken as positive) along the magnetic field. See the top panel of Fig. 1 for the flow frame setup. In order to interpret the beam instability in the observer frame (representative to the spacecraft frame), the Galilean transformation is introduced with a flow speed U_{f} (taken as negative, in the opposite direction to the beam). The beam velocity reduces to $U_{\mathrm{f}} + U_{\mathrm{b}}$ (see bottom panel of Fig. 1). The observer frame may also be regarded as the shock frame such that the beam velocity is $U_{\mathrm{f}} + U_{\mathrm{b}}$ with respect to the bow shock.

2.2 Analysis in the flow frame

The right-hand resonant instability represents an energy and momentum transfer of the beam ions into the electromagnetic waves. The kinetic treatment of the beam instabilities is documented in the framework of linear Vlasov theory by Gary (1993).

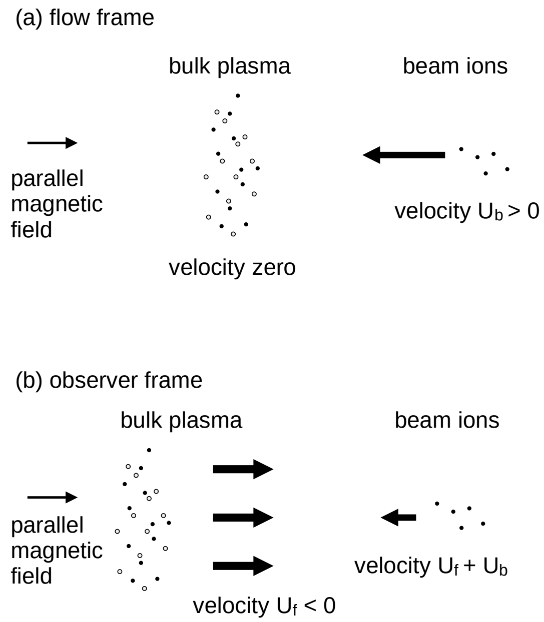

Figure 1. Ion beam injected into the bulk plasma in the flow frame (top) and in the observer frame (bottom).

Single and multi-spacecraft observations in the Earth foreshock region confirm the right-hand resonant instability (Watanabe and Terasawa, 1984; Eastwood et al., 2003; Narita et al., 2003).

The right-hand resonant instability occurs when the low-frequency whistler mode (R+ branch) meets the beam resonance condition. The resonance occurs at a frequency below or around the ion cyclotron frequency. Figure 2 illustrates the dispersion relation diagram of four branches of electromagnetic waves, R^{+} the right-hand polarized parallel-propagating mode (whistler mode with positive helicity), R^{-} the left-hand polarized anti-parallel-propagating mode (ion-cyclotron mode with positive helicity), L^{+} the left-hand polarized parallel-propagating mode (ion-cyclotron mode with negative helicity), and L^{-} the right-hand polarized anti-parallel propagating mode (whistler mode with negative helicity). The symbols R and L represent the dielectric response or the wave helicity (spatial field rotation sense around the mean magnetic field), and the plus and minus signs represent the propagation direction with respect to the mean magnetic field.

The task is to find the crossing frequency between the R+ branch and the resonance condition. The low-frequency part of whistler dispersion relation for parallel propagation in a low-beta plasma (cold plasma) is, by including the effect of Hall current, is obtained after Hasegawa and Uberoi (Eq. 2.24 in 1982) or Gary (Eq. 6.2.5 in 1993) as

$$\frac{\omega}{\Omega_{\mathrm{i}}} \simeq \frac{k_{\parallel} V_{\mathrm{A}}}{\Omega_{\mathrm{i}}}\left(1+\frac{k_{\parallel} V_{\mathrm{A}}}{\Omega_{\mathrm{i}}}\right)^{1/2} \tag{1}$$

$$\simeq \frac{k_{\parallel} V_{\mathrm{A}}}{\Omega_{\mathrm{i}}}+\frac{1}{2}\left(\frac{k_{\parallel} V_{\mathrm{A}}}{\Omega_{\mathrm{i}}}\right)^{2}. \tag{2}$$

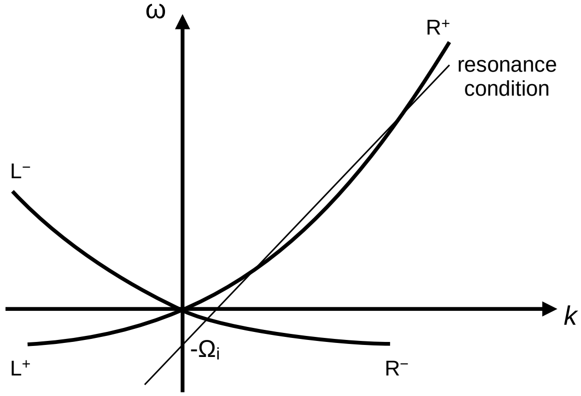

Figure 2. Dispersion relations and the beam resonance condition. Protons are assumed for the bulk ions and the beam ions with the cyclotron frequency $\Omega_{\rm i}$. The wave modes are the whistler wave propagating forward to the mean magnetic field (R+ mode) and backward (L- mode) and the ion cyclotron wave propagating forward (L+ mode) and backward (R- mode). The symbols R and L refer to the polarization, i.e., dielectric response in the Stix notation, and the plus and minus signs refer to the propagation sense with respect to the mean magnetic field. The beam resonance condition is indicated by the thin line, and intersects the y-axis (long wavelength limit) the ion cyclotron frequency in the negative frequency domain. The beam resonance with the R+ mode is considered here. The resonance with the R- mode is unlikely because of the opposite group velocity direction to the beam (no sufficient time for the energy exchange).

The resonance condition for the beam ions (assumed to be protons) is expressed as

$$\omega - k_{\|} U_{\rm b} = -\Omega_{\rm i}. \tag{3}$$

Here ω denotes the wave frequency, k the parallel wavenumber to the mean magnetic field, $V_{\rm A}$ the Alfvén speed, and $\Omega_{\rm i}$ the ion cyclotron frequency for protons.

For an easier theoretical treatment, we normalize the frequency to the ion cyclotron frequency (for the protons) $\Omega_{\rm i}$, and rewrite hereafter the normalized frequency as $\tilde{\omega} = \omega/\Omega_{\rm i}$. The proton cyclotron frequency is then expressed as unity, $\tilde{\Omega}_{\rm i} = 1$. The wavenumber is accordingly normalized to the ion inertial length $V_{\rm A}/\Omega_{\rm i}$ and we rewrite the normalized wavenumber as $\tilde{k} = k V_{\rm A}/\Omega_{\rm i}$. The same normalization applies to the parallel wavenumber. When limiting to the parallel propagation, the whistler dispersion relation (Eq. 1) and the resonance condition are rewritten as

$$\tilde{\omega} = \tilde{k}_{\|} + \frac{1}{2}\tilde{k}_{\|}^2. \tag{4}$$

and

$$\tilde{\omega} - \tilde{k}_{\|}\tilde{U}_{\rm b} = -1, \tag{5}$$

respectively. The beam velocity is normalized to the Alfvén speed as $\tilde{U}_{\rm b} = U_{\rm b}/V_{\rm A}$.

By eliminating the frequency ω in Eqs. (4) and (5), we obtain the quadratic equation as to the resonance wavenumber,

$$\tilde{k}_{\|}^2 - 2(\tilde{U}_{\rm b} - 1)\tilde{k}_{\|} + 2 = 0. \tag{6}$$

The roots of Eq. (6) are

$$\tilde{k}_{\parallel} = \tilde{U}_{\mathrm{b}} - 1 \pm \sqrt{(\tilde{U}_{\mathrm{b}} - \tilde{U}_{-})(\tilde{U}_{\mathrm{b}} - \tilde{U}_{+})} \quad (7)$$

$$\tilde{U}_{\pm} = 1 \pm \sqrt{2} \quad (8)$$

For the existence of real-number solution, the beam velocity must satisfy the condition

$$\tilde{U}_{\mathrm{b}} \geq \tilde{U}_{+} = 1 + \sqrt{2} \quad (9)$$

Interestingly, the threshold value is about $1+\sqrt{2} \sim 2.4$, which is close to the critical Alfvén Mach number for the shock reflection mechanism. The wave-particle interaction is considered to sufficiently scatter the particles in a low Mach number shock up to an Alfvén Mach number of about 2.7 (sub-critical shocks). In a high Mach number shock (Alfvén Mach number above 2.7), the dissipation is primarily made by the specular reflection by the cross-shock potential and the wave-particle interactions at the shock transition. Our theory predicts that the critical beam Mach number is about 2.4. There might be a relation between the dissipation mechanism and the ion beam instability in the collisionless shock such that the beam instability potentially contributes to a more efficient shock dissipation.

The lower wavenumber solution of Eq. (7) with the minus sign is the resonance wavenumber of interest. The higher wavenumber solution is valid for a lower beam velocity near the "touch point" (Eq. 9), but may not be exact for a higher beam velocity as the parabolic approximation of the whistler mode is no longer valid at higher frequencies. The resonance frequency in the flow frame is derived from Eq. (5) as

$$\omega = \left(\tilde{U}_{\mathrm{b}} - 1 - \sqrt{(\tilde{U}_{\mathrm{b}} - \tilde{U}_{-})(\tilde{U}_{\mathrm{b}} - \tilde{U}_{+})}\right) \tilde{U}_{\mathrm{b}} - 1 \quad (10)$$

2.3 Transformation into the observer frame

By introducing the Doppler shift by the bulk flow as $\tilde{k}_{\parallel}\tilde{U}_{\mathrm{f}}$ (here $\tilde{U}_{\mathrm{f}}$ denotes flow speed in units of the Alfvén speed) in the opposite direction to the beam velocity and transforming the frequency from the flow rest frame into the observer frame, we obtain the resonance frequency $\tilde{\omega}'$ (in units of the proton cyclotron frequency) as

$$\tilde{\omega}' = \tilde{k}_{\parallel}(\tilde{U}_{\mathrm{b}} + \tilde{U}_{\mathrm{f}}) - 1 \quad (11)$$

$$= \left[(\tilde{U}_{\mathrm{b}} - 1) - \sqrt{(\tilde{U}_{\mathrm{b}} - \tilde{U}_{-})(\tilde{U}_{\mathrm{b}} - \tilde{U}_{+})}\right] \times (\tilde{U}_{\mathrm{b}} + \tilde{U}_{\mathrm{f}}) - 1 \quad (12)$$

Figure 3 left column displays the dispersion relation and the resonance condition in the comoving frame and the observer frame for the foreshock ions with a beam velocity of $\tilde{U}_{\mathrm{b}} = 7$ and a flow speed of $\tilde{U}_{\mathrm{f}} = -5$. Whistler wave frequencies are transformed into the negative frequency domain while retaining the wavenumber. The temporal sense of wave field rotation (polarization) changes accordingly from right-hand rotation around the magnetic field into left-hand rotation.

Figure 3 right column displays the dispersion relation and the resonance condition for a beam velocity canceling the flow speed $\tilde{U}_{\mathrm{b}} = -\tilde{U}_{\mathrm{f}} = 5$ for the pickup ion scenario. The resonance frequency is the ion cyclotron frequency with left-hand sense of field rotation in the observer frame.

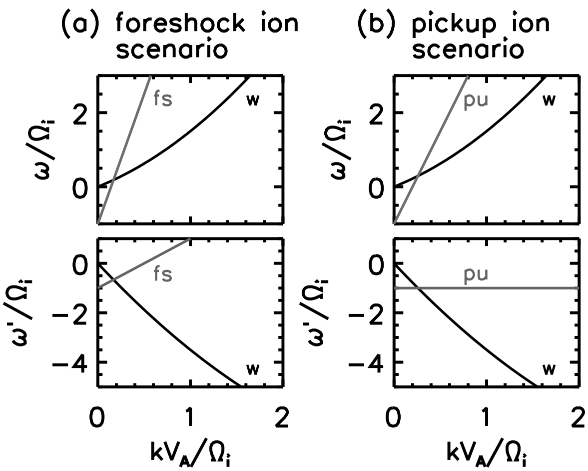

Figure 3. Whistler dispersion relation (in black) and beam resonance condition (in gray) in the comoving frame with the flow (top panels) and the observer frame standing in the flow (bottom panels). A beam velocity of $U_\mathrm{b}/V_\mathrm{A} = 7$ and a flow speed of $U_\mathrm{f}/V_\mathrm{A} = -5$ are chosen for the foreshock ion scenario (left column). The beam velocity canceling the flow speed is chosen for the pickup ion scenario (right column), $U_\mathrm{b}/V_\mathrm{A} = -U_\mathrm{f}/V_\mathrm{A} = 5$.

Equation (12) relates the resonance frequency (e.g., peak of the magnetic power spectrum in the spacecraft frame) with the beam velocity and the flow speed. The frequency estimate (Eq. 12) indicates that the ion cyclotron frequency is expected for the beam instability for the pickup ions by substituting the sign-reversed flow speed into beam velocity as $\tilde{U}_\mathrm{b} = -\tilde{U}_\mathrm{f}$ (pickup ion cyclotron waves).

3 Velocity estimate

Equation (12) may be regarded as a function of the beam velocity in the flow frame $\tilde{U}_\mathrm{b}$ and the flow speed $\tilde{U}_\mathrm{f}$ given that the frequency is known in the observer frame. A useful tool can be developed from Eq. (12). that is, we derive the relation between the beam velocity in the observer frame $\tilde{U}'_\mathrm{b}$ defined as

$$\tilde{U}'_\mathrm{b} = \tilde{U}_\mathrm{b} + \tilde{U}_\mathrm{f} \tag{13}$$

and the flow speed $\tilde{U}_\mathrm{f}$ for the resonance frequency $\tilde{\omega}'$. We can derive the expression of $\tilde{U}_\mathrm{b}$ by transforming Eq. (12) into

$$\frac{\tilde{\omega}'+1}{\tilde{U}'_\mathrm{b}} - (\tilde{U}_\mathrm{b} - 1) = -\sqrt{(\tilde{U}_\mathrm{b} - \tilde{U}_-)(\tilde{U}_\mathrm{b} - \tilde{U}_+)} \tag{14}$$

and squaring Eq. (14) as

$$\left[\frac{\tilde{\omega}'+1}{\tilde{U}'_\mathrm{b}} - (\tilde{U}_\mathrm{b} - 1)\right]^2 = (\tilde{U}_\mathrm{b} - \tilde{U}_-)(\tilde{U}_\mathrm{b} - \tilde{U}_+). \tag{15}$$

Equation (15) is simplified to

$$\tilde{U}_{\rm b} = \frac{\tilde{\omega}'+1}{2\tilde{U}'_{\rm b}} + \frac{\tilde{U}'_{\rm b}}{\tilde{\omega}'+1} + 1. \tag{16}$$

We combine Eq. (16) with Eq. (13), and obtain $\tilde{U}_{\rm f}$ as a function of $\tilde{U}'_{\rm b}$ as

$$\tilde{U}_{\rm f} = -\frac{\tilde{\omega}'+1}{2\tilde{U}'_{\rm b}} + \left(1 - \frac{1}{\tilde{\omega}'+1}\right)\tilde{U}'_{\rm b} - 1. \tag{17}$$

Figure 4 is the graphical representation of Eq. (17) at various values of $\tilde{\omega}'$. Three conditions are imposed for $\tilde{U}_{\rm f}$ and $\tilde{U}'_{\rm b}$: First, the flow is in the negative direction (opposite direction to the beam) in the observer frame, so $\tilde{U}_{\rm f} < 0$. Second, the beam velocity is in the positive direction in the observer frame for the formation of the foreshock region, so $\tilde{U}'_{\rm b} > 0$. Third, the beam resonance must occur, so $\tilde{U}_{\rm b} > \tilde{U}_+$ in the flow frame (cf. Eq. 9), which is transformed into $\tilde{U}_{\rm f} < \tilde{U}'_{\rm b} - U_+$ in the observer frame. The velocity diagram shows the relation between the flow speed and the beam velocity if the resonance frequency is set or known. The flow speed has a positive slope to smaller values of beam velocity (typically $\tilde{U}'_{\rm b} \lesssim 0.5$), while the slope becomes negative at larger values of beam velocity ($\tilde{U}'_{\rm b} \gtrsim 0.5$).

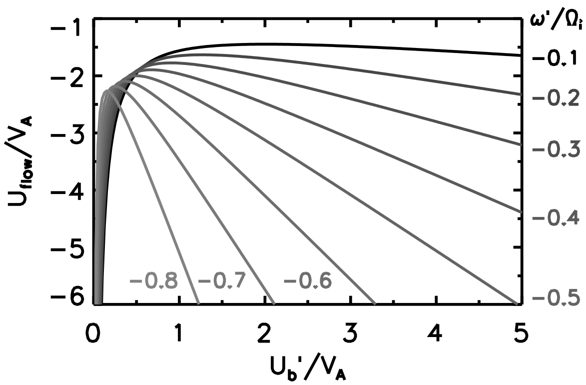

Figure 4. Velocity diagram showing the flow speed (normalized to the Alfvén speed) $U_{\rm f}/V_{\rm A}$ as a function of the beam velocity (also normalized to the Alfvén speed) in the observer frame $\tilde{U}'_{\rm b}/V_{\rm A}$ at different values of the resonance frequency (normalized to the proton cyclotron frequency) in the observer frame $\tilde{\omega}'/\Omega_{\rm i}$.

One can develop a useful tool from Eq. (17) and the knowledge from the Earth foreshock studies, since the beam velocity is nearly the same as the Alfvén speed in the flow rest frame (Narita et al., 2003). We determine the flow speed as a function of the observer-frame frequency at several representative values of beam velocity (in the observer frame), and plot the diagram in Fig. 5. For the beam velocity of the order of Alfvén speed or higher,, $U'_{\rm b} \gtrsim V_{\rm A}$, the estimated flow speed is a monotonous function of the observer-frame frequency. The flow velocity increases more rapidly at higher frequencies (typically $\omega'/\Omega_{\rm i} \gtrsim 0.4$). Figure 5 gives us a range of of the estimated flow speed if the range of beam velocity is set.

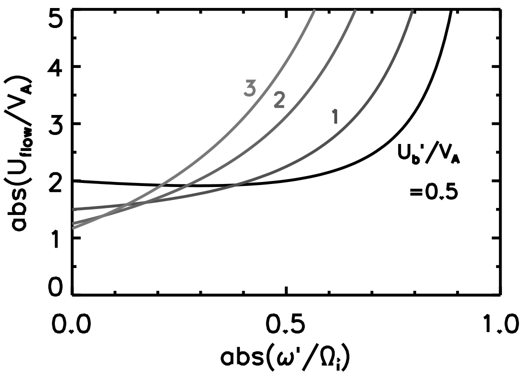

Figure 5. Flow speed diagram as a function of the resonance frequency in the observer frame at different beam velocities. Absolute values of the frequency and the flow speed are used in the plot.

4 Discussion

4.1 Validity of the model

We constructed our beam instability model under the non-relativistic, low-frequency, and low-beam-density conditions. We discuss the validity of the model in the following.

1. **Galilean approximation.**

   The solar wind speed is about 400 $\mathrm{km\,s^{-1}}$ at the distance of Mercury orbit (0.3 to 0.4 astronomical units). The back-streaming ion beam velocity is in the range from 500 to 1000 $\mathrm{km\,s^{-1}}$ (e.g., Glass et al., 2023). In total, the velocity of up to 1500 $\mathrm{km\,s^{-1}}$ is the likely range of the velocities considered in our model. The ratio of the velocity to the speed of light (Lorentz factor beta) is estimated as $\beta = 0.005$, and the Lorentz factor gamma is $\gamma = 1.0000125$. The Galilean approximation is sufficient in our model. See Appendix B for the relativistic treatment.

2. **Low-frequency approximation.**

   Our model breaks down at shorter wavelengths (higher wavenumbers) because the second-order Taylor expansion (parabolic fitting) of the whistler dispersion relation is no longer valid at shorter wavelengths. Our model is valid at a wavelength (of the low-frequency whistler mode) from MHD scales (typically about 1000 km and above in the solar wind) down to about the ion inertial length (down to about 100 km).

3. **Low beam density.**

   Our model is valid for a low-density of beam ions (typically below 0.1 % of the bulk ion density). When the beam density is higher, the resonance condition changes in two folds. First, the beam resonance occurs at a wider range of wavenumbers (the growth rate has a finite width in the wavenumber domain) around the resonance wavenumber (the minus sign version of Eq. 8). Second, the firehose instability sets on by the beam contributing to the dynamic pressure parallel to the mean magnetic field. The beam-firehose instability occurs in the MHD regime such that the R and L modes are not yet dispersive in the long wavelength limit.

4.2 Deviation from parallel propagation

Smaller angular misalignment of the wave propagation direction from the mean magnetic field has no significant impact on the resonance condition. Qualitatively speaking, obliquely-propagating whistler mode waves are elliptically polarized and thus have both right-hand and left-hand polarized components. The elliptic polarization implies the possibility of the beam resonance no only with the right-hand component but also with the left-hand component. The transition into the left-hand beam resonance occurs, however, at a larger propagation angle 45 to 60 degrees to the mean magnetic field (Verscharen and Chandran, 2013; Narita and Motschmann, 2025).

Figure 6 displays the dispersion relations and the growth rate for parallel propagation angles of $\theta_{kB} = 0°$, $10°$, and $20°$, The unstable mode has no practical difference in the wavenumber domain ($0.25 \le kc/\omega_{\mathrm{pi}} \le 0.28$) between the case of $\theta_{kB} = 0°$ and that of $\theta_{kB} = 10°$. The wavenumber range of the unstable mode slightly becomes higher at $\theta_{kB} = 20°$ ($0.26 \le kc/\omega_{\mathrm{pi}} \le 0.29$).

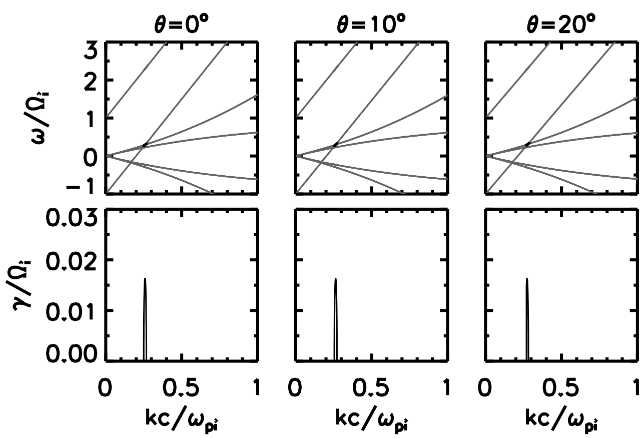

Figure 6. Linear instability analysis using the cold plasma dielectric tensor for a wave propagation angle of 0 degree, 10 degree, and 20 degree to the mean magnetic field.

4.3 Magnetic field oblique to the bulk flow

The model can be upgraded to a mean magnetic field oblique to the bulk flow direction by projecting the flow velocity onto the the mean magnetic field, The Doppler shift term changes from $\tilde{k}_{\|}\tilde{U}_{\mathrm{f}}$ into $\tilde{k}_{\|}\tilde{U}_{\mathrm{f}}\cos\theta$, where θ is the angle between the flow direction and the axis of the mean magnetic field. A smaller value of the angle is used from the mean field direction or the opposite direction to the mean field such that the projection does not change the sign, $0 \le \cos\theta \le 1$.

4.4 Heavier ion species

The Mercury plasma environment has heavier ions other than protons. Examples are helium alpha particles (He^{++}) of the solar wind origin and molecular or atomic species of the exospheric origin such as H_2^+, Li^+, and Na^+:

- The helium alpha particles stream in the anti-sunward direction. The alpha particles may have a different flow speed from the bulk flow speed in the solar wind (electron-proton plasma), and can potentially drive the beam instability by resonating with the whistler or the ion-cyclotron mode (e.g., Verscharen and Chandran, 2013), but this instability scenario is intrinsic to the solar wind. Specular reflection of the helium alpha particles at the shock is unlikely because the protons are most easily accelerated by the electrostatic shock potential back to the solar wind to form the foreshock region. The backstreaming alpha particles have so far not yet been reported in the shock-upstream region.

- Exospheric particles may be present in the shock-upstream region. The beam velocity is so small (cf. the escape velocity is about 4 $\mathrm{km\,s^{-1}}$ at Mercury) compared to the solar wind speed (about 400 $\mathrm{km\,s^{-1}}$) that the waves driven by the beam instability appear as the pickup ion-cyclotron wave. In this scenario, it is impossible to estimate the flow speed because the frequency is the ion cyclotron frequency in the observer frame.

We can nevertheless generalize the instability model to the beam of heavier ion species. Equation (5) is generalized into

$$\tilde{\omega} - \tilde{k}_{\parallel}\tilde{U}_{\mathrm{b}} = -\frac{1}{n}, \tag{18}$$

where we have introduced the mass-per-charge factor by n. For example, the alpha particles He^{++} are characterized by the normalized cyclotron frequency $1/2$ (so $n=2$), the helium singular ionized state by the frequency $1/4$ ($n=4$), and so on. Combination of Eq. (18) with Eq. (4) gives the resonance wavenumber as

$$\tilde{k}_{\parallel} = \tilde{U}_{\mathrm{b}} - 1 - \sqrt{(\tilde{U}_{\mathrm{b}}-1)^2 - \frac{2}{n}} \tag{19}$$

and the resonance frequency in the observer frame as

$$\tilde{\omega}' = \left[\tilde{U}_{\mathrm{b}} - 1 - \sqrt{(\tilde{U}_{\mathrm{b}}-1)^2 - \frac{2}{n}}\right](\tilde{U}_{\mathrm{b}} + \tilde{U}_{\mathrm{f}}) - \frac{1}{n}. \tag{20}$$

The resonance wavenumber and the resonance frequency approach to zero ($\tilde{k}_{\parallel} \to 0$ and $\tilde{\omega}' \to 0$) for a larger value of the mass-per-charge factor, $n \to \infty$. For the pickup ions, the beam velocity is the flow velocity with the opposite sign, and $\tilde{U}_{\mathrm{b}} + \tilde{U}_{\mathrm{f}} = 0$ holds. The resonance frequency in the observer frame is then $\tilde{\omega}' = -1/n$.

5 Concluding remarks

Our ion beam instability model determines the resonance frequency and wavenumber by equating the low-frequency whistler dispersion relation with the beam resonance condition in favor of planetary foreshock wave excitation. The resonance is of right-hand type in favor of $R+$ mode (whistler branch), and occurs at a beam velocity of at least $\tilde{U}_{\mathrm{b}} = 1+\sqrt{2} \sim 2.4$ in the flow rest frame. The instability condition is likely satisfied in the near-Mercury solar wind as the Mach number is mostly above 4 after the MESSENGER observation and the ENLIL calculation (Winslow et al., 2013). It is interesting to note that the critical beam velocity $\tilde{U}_\mathrm{b} \sim 2.4$ roughly coincides with the critical Alfvén Mach number for the specular reflection at the collisionless shocks (which is about 2.7).

Our model is capable of predicting the wavelength and the frequency for the beam instability for the given set of beam velocity and flow speed. Here is an example. For a beam velocity of $\tilde{U}'_\mathrm{b} = 1$ in the observer frame and a flow Mach number of 6 in the opposite direction to the beam $\tilde{U}_\mathrm{f} = -6$ (e.g., Winslow et al., 2013), we obtain the beam velocity in the flow frame as $\tilde{U}_\mathrm{b} = \tilde{U}_\mathrm{b} + \tilde{U}_\mathrm{f} = 7$. The resonance wavenumber is estimated as $k_\| V_\mathrm{A}/\Omega_\mathrm{i} \simeq 0.17$ (Eq. 7) and the frequency as $\omega'/\Omega_\mathrm{i} \simeq -0.83$ (Eq. 11). By referring to the magnetic field statistics of about 20 nT (Romanelli and DiBraccio, 2021) and the ion density of about 40 cm^{-3} (Winslow et al., 2013), we obtain an Alfvén speed of $V_\mathrm{A} \simeq 70$ km s^{-1} and an ion inertial length of $V_\mathrm{A}/\Omega_\mathrm{i} \simeq 3.7$ km rad^{-1}. The resonance wavelength is thus estimated as 3.5 km and the frequency as 2.5 s^{-1}, which is well within the sampling rate of the fluxgate magnetometer on-board the BepiColombo Mio spacecraft with 128 Hz for the burst mode or H mode, and 8 Hz for the normal mode or M1 mode (Baumjohann et al., 2020). The backstreaming ions are observed by MESSENGER (e.g., Glass et al., 2023) The pickup ion cyclotron waves are also observed by MESSENGER (e.g., Schmid et al., 2022) Combination of Mio MGF and Mio MPPE/MIA instrument is ideally suited to test for our instability model against the spacecraft data.

Our model is developed for a one-dimensional setup, that is, the beam velocity, the flow, and the wave propagation are assumed to be all aligned with the mean magnetic field. Even though such an aligned situation is most likely realized in the Mercury upstream region as the Parker spiral angle is the smallest (most radial) of all the solar system planets, our model may be upgraded to a weakly misaligned wave system (like the effect of inclination of the mean magnetic field to the flow direction or a moderately oblique propagation angle to the mean magnetic field) by projecting the misaligned system onto our one-dimensional treatment.

Code and data availability. The dispersion solver used for generating Fig. 6 is available upon request to the authors.

Appendix A: Dispersion relation

Dispersion relation for low-frequency, parallel-propagating whistler waves in an electron-ion plasma is shown in various forms in literature, such as Eq. (6.2.5) in Gary (1993) and Eq. (2.24) in Hasegawa and Uberoi (1982). We start with the general form of the R-mode dispersion relation for the two-component cold plasma (electrons and ions), that is,

$$\omega^2 - k^2 c^2 - \frac{\omega\,\omega_\mathrm{pe}^2}{\omega + \Omega_\mathrm{e}} - \frac{\omega\,\omega_\mathrm{pi}^2}{\omega + \Omega_\mathrm{i}} = 0, \tag{21}$$

where ω denotes the frequency, k the wavenumber (parallel to the mean magnetic field), c the speed of light, ω_pe the electron plasma frequency, ω_pi the ion plasma frequency, Ω_e the electron cyclotron frequency, and Ω_i the ion cyclotron frequency. See Eq. (6.2.4) in Gary (1993) for the derivation of Eq. (21).

We now apply the low-frequency approximation. First, we neglect the first term, ω^2 , on l.h.s. of Eq. (21). Second, the denominator of the third term on l.h.s. of Eq. (21) is simplified into Ω_e. We then obtain the dispersion relation as

$$k^2c^2 = -\frac{\omega\,\omega_\mathrm{pe}^2}{\Omega_\mathrm{e}} - \frac{\omega\,\omega_\mathrm{pi}^2}{\Omega_\mathrm{i}}\frac{1}{1+\frac{\omega}{\Omega_\mathrm{i}}} \tag{22}$$

$$= -\frac{\omega\,\omega_\mathrm{pe}^2}{\Omega_\mathrm{e}} - \frac{\omega\,\omega_\mathrm{pi}^2}{\Omega_\mathrm{i}}\left[1-\frac{\omega}{\Omega_\mathrm{i}}+\left(\frac{\omega}{\Omega_\mathrm{i}}\right)^2\right] \tag{23}$$

$$= -\omega\left(\frac{\omega_\mathrm{pe}^2}{\Omega_\mathrm{e}}+\frac{\omega_\mathrm{pi}^2}{\Omega_\mathrm{i}}\right)+\frac{\omega^2\,\omega_\mathrm{pi}^2}{\Omega_\mathrm{i}^2}-\frac{\omega^3\,\omega_\mathrm{pi}^2}{\Omega_\mathrm{i}^3}. \tag{24}$$

Note that the second-order Taylor expansion is used in deriving Eq. (23).

We introduce the charge neutrality of the plasma, which cancels the first term on r.h.s. in Eq. (24). The charge neutrality reads in the frequency form as

$$\frac{\omega_\mathrm{pe}^2}{\Omega_\mathrm{e}}+\frac{\omega_\mathrm{pi}^2}{\Omega_\mathrm{i}} = \frac{q_\mathrm{e}n_\mathrm{e}+q_\mathrm{i}n_\mathrm{i}}{\epsilon_0 B_0} = 0, \tag{25}$$

where q_e and q_i denote the electron and ion charges including the sign, and n_e and n_i the the number density of electrons and ions, ϵ_0 the permittivity of free space, and B_0 the magnetic field magnitude. We also rewrite the squared frequency ratio $\omega_\mathrm{i}^2/\Omega_\mathrm{i}^2$ into

$$\frac{\omega_\mathrm{pi}^2}{\Omega_\mathrm{i}^2} = \frac{c^2}{V_\mathrm{A}^2}, \tag{26}$$

where V_A denotes the Alfvén speed. Combining Eqs. (24)–(26), we obtain the dispersion relation as

$$k^2c^2 = \omega^2\frac{c^2}{V_\mathrm{A}^2}\left(1-\frac{\omega}{\Omega_\mathrm{i}}\right). \tag{27}$$

When introducing the phase speed as

$$v_\mathrm{ph} = \frac{\omega}{k}, \tag{28}$$

the dispersion relation is formulated as

$$v_\mathrm{ph}^2 = \frac{V_\mathrm{A}^2}{1-\frac{\omega}{\Omega_\mathrm{i}}}, \tag{29}$$

which is further simplified by Taylor-expanding the fraction to the first order as

$$v_\mathrm{ph}^2 \simeq V_\mathrm{A}^2\left(1+\frac{\omega}{\Omega_\mathrm{i}}\right), \tag{30}$$

which reproduces Eq. (2.24) in Hasegawa and Uberoi (1982).

Using the fact that the low-frequency whistler wave roughly satisfies the dispersion relation for the Alfvén wave,

$$\omega \simeq kV_\mathrm{A}, \tag{31}$$

Equation (30) is written in the form of

$$\frac{\omega^2}{k^2} = V_{\rm A}^2\left(1+\frac{kV_{\rm A}}{\Omega_{\rm i}}\right) \quad (32)$$

$$= V_{\rm A}^2\left(1+\frac{kc}{\omega_{\rm pi}}\right), \quad (33)$$

which reproduces Eq. (6.2.5) in Gary (1993). Note that the ion inertial length is introduced in Eqs. (32)–(33) through Eq. (26).

Appendix B: Relativistic beam resonance

Quantitatively speaking, the relativistic effect modifies the cyclotron frequency in the resonance condition as follows:

$$\omega - k_\parallel U_{\rm b} = \frac{\Omega_{\rm i}}{\gamma}. \quad (34)$$

Equation (34) is obtained by re-formulating Eq. (3) into the relativistic covariant form as

$$\Lambda^0{}_\mu k^\mu = k'^0, \quad (35)$$

where the four-wavevectors k^μ (in the rest frame of bulk plasma) and k'^ν (in the rest frame of the beam) are defined as

$$k^\mu = (\omega/c, k_\parallel, 0, 0) \quad (36)$$

$$k'^\nu = (\Omega_{\rm i}/c, k'_\parallel, 0, 0) \quad (37)$$

and the Lorentz transformation matrix $\Lambda^\nu{}_\mu$ as

$$\Lambda^\nu{}_\mu = \begin{bmatrix} \gamma & -\gamma\beta & 0 & 0 \\ -\gamma\beta & \gamma & 0 & 0 \\ 0 & 0 & 1 & 0 \\ 0 & 0 & 0 & 1 \end{bmatrix} \quad (38)$$

with the Lorentz factors $\beta = U_{\rm b}/c$ and $\gamma = (1-U_{\rm b}^2/c^2)^{-1/2}$.

Author contributions. All authors listed have made a substantial, direct, and intellectual contribution to the work and approved it for publication.

Competing interests. Conflict of Interest: The authors declare that the research was conducted in the absence of any commercial or financial relationships that could be construed as a potential conflict of interest.

Acknowledgements. We acknowledge the funding assist by German Science Foundation under project number 535057280.

References

Baumjohann, W., Matsuoka, A., Narita, Y., Magnes, W., Heyner, D., Glassmeier, K.-H., Nakamura, R., Fischer, D., Plaschke, F., Volwerk, M., Zhang, T L., Auster, H.-U., Richter, I., Balogh, A., Carr, C. M., Dougherty, M., Horbury, T. S., Tsunakawa, H., Matsushima, M., Shinohara, M., Shibuya, H., Nakagawa, T., Hoshino, M., Tanaka, Y., Anderson, B. J., Russell, C. T., Motschmann, U., Takahashi, F., and Fujimoto, A., The BepiColombo–Mio magnetometer en route to Mercury, Space Sci. Rev., 216, 125, 2020. https://doi.org/10.1007/s11214-020-00754-y

Benkhoff, J., Murakami, G., Baumjohann, W., Besse, S., Bunce, E., Casale, M., Cremosese, G., Glassmeier, K.-H., Hayakawa, H., Heyner, D., Hiesinger, H., Huovelin, J., Hussmann, H., Iafolla, V., Iess, L., Kasaba, Y., Kobayashi, M., Milillo, A., Mitrofanov, I. G., Montagnon, E., Novara, M., Orsini, S., Quemerais E., Reininghaus, U., Saito, Y., Santoli, F., Stramaccioni, D., Sutherland, O., Thomas, N., Yoshikawa, I., and Zender, J., BepiColombo – Mission Overview and Science Goals. Space Sci. Rev., 217, 90, 2021. https://doi.org/10.1007/s11214-021-00861-4

Delva, M., Mazelle, C., Bertucci, C., Volwerk, M., Vörös, Z., and Zhang, T. L., Proton cyclotron wave generation mechanisms upstream of Venus. J. Geophys. Res. Space Physics, 116, A02318, 2011. https://doi.org/10.1029/2010ja015826

Delva, M., Mazelle, C., and César, B., Upstream Ion Cyclotron Waves at Venus and Mars, Space Sci. Rev., 162, 5–24, 2011. https://doi.org/10.1007/s11214-011-9828-2

Eastwood, J. P., Balogh, A., Lucek, E. A., Mazelle, C., and Dandouras, I., On the existence of Alfvén waves in the terrestrial foreshock, Ann. Geophys., 21, 1457–1465, 2003. https://doi.org/10.5194/angeo-21-1457-2003

Gary, S. P., Theory of Space Plasma Microinstabilities, Cambridge University Press, 1993. https://doi.org/10.1017/CBO9780511551512

Glass, A. N., Tracy, P. J., Raines, J. M., Jia, X., Romanelli, N., and DiBraccio, G. A. Characterization of Foreshock Plasma Populations at Mercury, J. Geophys. Res. Space Physics, 128, e2022JA031111, 2023. https://doi.org/10.1029/2022JA031111

Hasegawa, A., and Uberoi, C., The Alfvén wave, DOE Critical Review Series, DOE/TIC-11197, Technical Information Center, U.S. Department of Energy, 1982. https://doi.org/10.2172/5259641

Le, G., Chi, P. J., Blanco-Cano, X., Boardsen, S., Slavin, J. A., Anderson, B. J., and Korth, H., Upstream ultra-low frequency waves in Mercury's foreshock region: MESSENGER magnetic field observations, J. Geophys. Res. Space Physics, 118, 2809–2823, 2013. https://doi.org/10.1002/jgra.50342

Narita, Y., Glassmeier, K.-H., Schäfer, S., Motschmann, U., Sauer, K., Dandouras, I., Fornaçon, K.-H., Georgescu, E., and Rème, H., Dispersion analysis of ULF waves in the foreshock using cluster data and the wave telescope technique, Geophys. Res. Lett., 30, 1710, 2003. https://doi.org/2003GL017432

Narita, Y., and Motschmann, U.: A rational view of the the beam instabilities, AIP Advances, 15, 055104 (2025). https://doi.org/10.1063/5.0263275

Romanelli, N., and DiBraccio, G. A., Occurrence rate of ultra-low frequency waves in the foreshock of Mercury increases with heliocentric distance, Nature Comm., 12, 6748, 2021. ttps://doi.org/10.1038/s41467-021-26344-2

Schmid, D. Lammer, H., Plaschke, F., Vorburger, A., Erkaev, N. V., Wurz, P., Narita, Y. Volwerk, M., Baumjohann, W., and Anderson, B. J., Magnetic evidence for an extended hydrogen exosphere at Mercury, J. Geophys. Res. Planets, 127, e2022JE007462, 2022. https://doi.org/10.1029/2022JE007462

Verscharen, D., and Chandran, B. D. G.: The dispersion relations and instability threshold of oblique plasma modes in the presence of an ion beam, Astrophys. J., 764, 88, 2013. https://doi.org/10.1088/0004-637X/764/1/88

Watanabe, Y., and Terasawa, T., On the excitation mechanism of the low-frequency upstream waves, J. Geophys. Res., 89, 6623–6630, 1984. https://doi.org/10.1029/JA089iA08p06623

Winslow, R. M., Anderson, B. J., Johnson, C. L., Slavin, J. A., Korth, H., Purucker, M. E., Baker, D. N., Solomon, S. C., Mercury's magnetopause and bow shock from MESSENGER Magnetometer observations, J. Geophys. Res. Space Physics, 118, 2213–2227, 2013. https://doi.org/10.1002/jgra.50237